Journal of Innovative Optical Health Sciences
Vol. 10, No. 6 (2017) 1742009 (12 pages)

DOI: 10.1142/S1793545817420093

Inverse elastographic method for analyzing the ocular lens compression test

Matthew A. Reilly*,†,§ and Andre Cleaver‡
*Department of Biomedical Engineering, The Ohio State University
Columbus, OH 43210, USA
†Department of Ophthalmology and Visual Science
The Ohio State University, Columbus, OH 43210, USA
‡Department of Mechanical Engineering, Tufts University
Medford, MA 02155, USA
§Reilly.196@osu.edu

Received 30 June 2017
Accepted 28 September 2017
Published 24 October 2017

The ocular lens stiffens dramatically with age, resulting in a loss of function. However, the mechanism of stiffening remains unknown, at least in part due to difficulties in making reliable measurements of the intrinsic mechanical properties of the lens. Recent experiments have employed manual compression testing to evaluate the stiffness of murine lenses which have genotypes pertinent to human lens diseases. These experiments compare the extrinsic stiffness of lenses from the genotype of interest to the wild-type lens in an effort to reach conclusions regarding the cellular or molecular basis of lens stiffening. However, these comparisons are confounded by alterations in lens size and geometry which invariably accompany these genetic manipulations. Here, we utilize manual lens compression to characterize the stiffness of a porcine lens and a murine lens. An inverse elastographic technique was then developed to estimate the intrinsic shear modulus of each lens as well as the elastic modulus of the lens capsule. The results were in good agreement with the previous literature values.

Keywords: Presbyopia; lens compression; lens mechanical properties; finite element analysis; lens biomechanics.

1. Introduction

The ocular lens is the pivotal tissue in accommodation — the primate eye's ability to alter its focal length.[1] This process uses biomechanical deformation of the lens to achieve a change in optical power.[2] Presbyopia is the progressive loss of accommodation amplitude with age and appears to arise due to an alteration in the biomechanical

§Corresponding author.

coupling of the lens and its capsule.[3,4] The clinical presentation of presbyopia coincides with the massive stiffening of the lens fiber cells, but it is unclear whether this is purely correlation, cause, or effect.[5] While it remains unclear whether this relationship is causal or correlative, accurate measurement of lens' mechanical properties may give important insights into potential mechanisms of lens stiffening and possibly presbyopia.

Considerable attention has been paid to the study of lens mechanics, invigorated by the application of finite element (FE) analysis to the study of accommodation and the accompanying conclusion that available mechanical properties were of insufficient quality to render useful predictions.[6] Previous methods for estimating lens stiffness include spinning tests,[7–9] dynamic mechanical analysis,[10] indentation,[11,12] penetration,[13] Brillouin microscopy,[14–19] acoustic methods,[20,21] and compression.[22–27] The lens capsule has been mechanically characterized by inflation testing[28,29] and uniaxial tensile testing.[30,31] However, no test has yet enabled a simultaneous mechanical analysis of both the lens and its capsule.

Mice are most often used as a model for lens-specific genetic manipulations, usually intended to study cataract (e.g., Refs. 32–34). Recently, they have also been used as a model for quantifying the contribution of specific proteins to lens mechanical properties by computing an extrinsic stiffness parameter derived from lens compression.[25,27] However, the use of an extrinsic mechanical property is inherently confounded by altered lens size and shape[35,36] — a common side effect of genetic manipulation.[37]

The intrinsic mechanical properties have been extracted from larger lenses (i.e., porcine and human) using spinning tests coupled with an inverse FE method.[8,9,38,39] However, the spinning test has not been successfully applied to mouse lenses due to size considerations. In the present study, we implement an inverse FE method for estimating the mechanical properties of porcine and murine lenses from a compression test. The experimental approach was designed to mimic similar compression tests performed by other groups (e.g., Refs. 22–27) while eliminating certain aspects which complicate the modeling process (e.g., the presence of a divet).

2. Materials and Methods

2.1. *Materials*

One young porcine eye was obtained from a local slaughterhouse and transported to the laboratory sealed in a plastic bag in a cooler on wet ice within 1 h post mortem. The lens was immediately dissected by opening the globe at the equator, then carefully separating the ciliary body using forceps. The lens was then placed in lens culture medium 199 (M199; Sigma-Aldrich; St. Louis, MO) and maintained at 37°C. The warm media and lens were placed on the lens compression system as described below. Following compression of the encapsulated lens, fine forceps were used to decapsulate the lens and it was again subjected to the compression protocol described below.

One eye from an adult wild-type (4.5 months; c57bl/6) mouse was obtained from another investigator immediately following humane euthanasia. Fine forceps were used to peel the sclera and other connective tissues away from the lens. Care was taken to ensure that the lens capsule was left intact to ensure that the lens itself was not damaged. The lens was placed in M199 and maintained at 37°C prior to compression.

All animal tissues were treated in compliance with institutionally-approved protocols.

2.2. *Lens compression apparatus*

Figure 1 shows the apparatus used to manually apply compression to the lens. A linear stage (6734K4 with 1/8″ pitch; McMaster-Carr; Aurora, OH) was manually manipulated to compress the lens while a voltmeter was used to record the output of a load cell with 20 g-force capacity (FSH02667; FUTEK Advanced Sensor Technology, Inc.; Irvine, CA). Flat aluminum plates were attached to the motion stage and the load cell. The load cell was calibrated using 1–20 g calibration masses (9048T41; McMaster-Carr) immediately prior to each experiment. This yielded a force resolution of 2 mg-force.

High-resolution digital photographs were taken using a digital camera (D810; Nikon Inc.; Melville, NY). A macro bellows (BALPRO; NOVOFLEX Präzisionstechnik GmbH; Memmingen, Germany) was used to allow high magnification imaging in conjunction with inverted lenses and appropriate

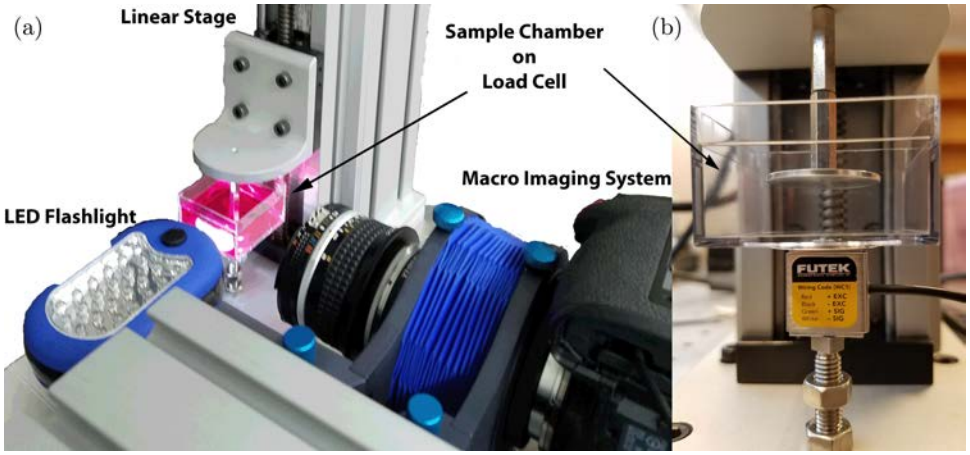

Fig. 1. (a) The lens compression apparatus and imaging system. The linear stage moves an aluminum plate vertically within the plastic sample chamber. (b): The sample chamber is mounted on the load cell, which is in turn rigidly connected to an optical table.

adapters. Scaling was determined by imaging high-precision ball bearings in the same focal plane immediately after the conclusion of each compression test. This yielded a spatial resolution of about $3\,\mu$m/px when imaging the porcine lens and 650 nm/px when imaging the murine lens.

2.3. *Mechanical testing protocol*

Preliminary experiments indicated significant water loss and adhesion between the aluminum plates and the lens when compression tests were performed in air. Therefore, the lens was placed in a rigid plastic container filled with lens culture medium 199 (M199; Sigma Aldrich; St. Louis, MO) heated to 37°C and placed on the lower plate of the compression apparatus. The lens was then photographed to allow construction of the unloaded geometry as described below. The load cell voltage was recorded and used as a baseline for all subsequent force measurements.

Once the initial conditions were established in this way, the upper plate was lowered into contact with the lens. Contact was determined as an increment in the least count of the voltmeter (i.e., an increase of at least 2 mg-force). Small increments of compression were then applied until the load cell voltage incremented. Photographs were taken at each increment. This process was repeated until lenses were compressed by about 15% of their original thickness.

Digital photographs were converted to binary masks by using the Quick Selection Tool in Photoshop CC 2015 (Adobe Systems; San Jose, CA). The location of edge pixels corresponding to the lens surface was extracted from these masks using MATLAB (r2016b; The Mathworks; Natick, MA). This allowed the construction of the computational model geometry as detailed below (Fig. 2). In addition, the fractional compression could be estimated based on the change in distance between the plates. Figure 3 gives force–displacement data for each test. Edge pixel locations and corresponding forces were then retained in increments of about 2.5% compression.

2.4. *Extrinsic stiffness estimation*

Previous experiments have reported the extrinsic measurements of lens stiffness for both porcine and murine lenses. Several of these fit a line to the force–displacement data, which are collected to about 10% axial compression, and report the slope of the line as the stiffness.[22,23,27] This approach was adopted here as well for the estimation of a "linear stiffness". Although the lens was loaded to ∼15% axial compression, only the initial 10% loading was used for estimating the linear stiffness.

Additionally, previous studies have characterized murine lenses to larger fractional compressions, then fit the resulting force–displacement data with an exponential function. The tangent to this exponential curve at various points may then be interpreted as the instantaneous stiffness.[24,25] This approach was also considered here by fitting all data with an exponential curve, then computing the

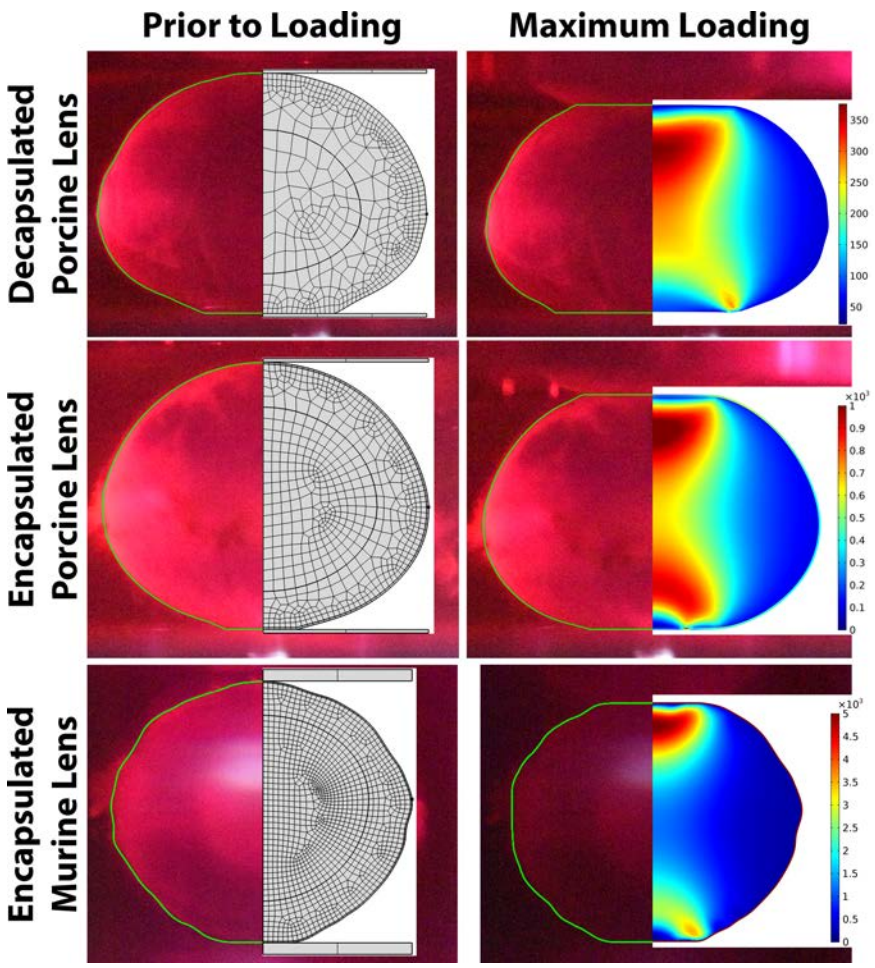

Fig. 2. Digital image analysis was used to identify edge pixels (green) in high-resolution photographs of the lenses before (left) and during (right) compression. Inset left: A quadrilateral mesh was generated automatically for each lens based on its unloaded geometry. Inset right: von Mises stresses (shown in Pa) generated in the lens during maximum compression for the optimized model.

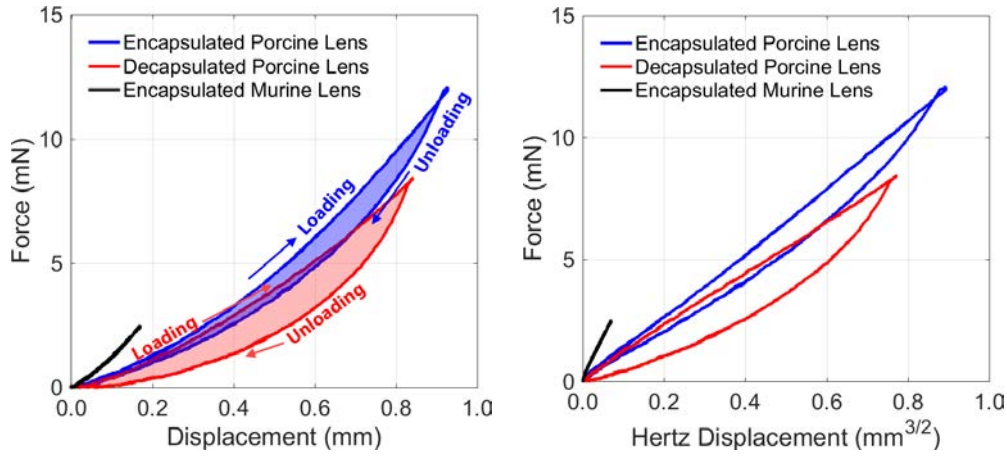

(a) (b)

Fig. 3. (a) Force–displacement curves for the young porcine and adult murine lenses. The encapsulated porcine lens is stiffer and has less hysteresis than the decapsulated porcine lens. Note the nonlinear shape of the curve arising from variable contact area. (b) The role of contact area is clarified by re-plotting the measurements in terms of the Hertz displacement (i.e., displacement raised to the 3/2 power), resulting in nearly straight lines for the loading curves.

tangent stiffness (i.e., the slope of the exponential force–displacement fitted curve) at zero and maximal strain.

2.5. *Analytical approach to estimating the shear modulus*

As a first approximation, the lens' shear modulus G was estimated using the contact theory of Hertz.[35,36] This theory can be modified to address the compression of a sphere with radius of curvature R between rigid parallel plates,[40] predicting that the force F and displacement δ are related by

$$F = \frac{8}{3}\frac{G(1+\nu)}{1-\nu^2}\sqrt{R}\delta^{3/2},$$

where ν is the Poisson ratio, assumed to be 0.5 (i.e., the lens was assumed to be incompressible). Values for R were previously reported as ~ 6 mm for the porcine lens[41,42] (average of anterior and posterior since both are in contact) and ~ 1 mm for the murine lens.[43] Linear regression thus allowed an estimate of G, assuming that the lens was mechanically homogeneous, using the data shown in Fig. 3. For encapsulated lenses, the contribution of the capsule was neglected (i.e., it was assumed to have the same shear modulus as the lens itself) when computing the Hertz modulus.

2.6. *Constructing the lens-specific model*

An axisymmetric FE model of each lens was constructed in COMSOL Multiphysics v5.2a (COMSOL, Inc.; Burlington, MA) based on the initial photograph of the unloaded lens (Fig. 2). Splines were used to describe the lens surface spanning the gap between the plates with anchor points located in angular increments of 4° from the optic axis with the origin at the intersection of the optic axis and the equatorial plane. When modeling an encapsulated lens, the capsule was added as a second spline interior to the lens surface. The distance of each anchor point from the corresponding lens surface anchor toward the origin was a constant amount corresponding to the capsular thickness (that is, the capsule thickness was assumed to be uniform across the entire lens surface). The thickness of the capsule was chosen as 57 μm for the porcine lens[30] and 12.8 μm for the adult murine lens.[44] The capsule was modeled as a neo-Hookean solid with a variable elastic modulus and a fixed Poisson ratio of 0.47.[28] The elastic modulus was estimated using the optimization procedure described below.

This geometry was automatically meshed (Fig. 2) using quadrilateral elements with localized refinement in the vicinity of contact (i.e., near the lens–plate interfaces). Meshes were iteratively refined until the resulting contact load at maximum compression varied by less than 1% from the previous mesh density. This final mesh density was then retained for all future simulations.

Compression was simulated using contact boundary conditions between the plates and the lens surface. A penalty method was adopted to ensure that the rigid plates did not penetrate the lens surface. The lower plate was held fixed while the experimentally-measured displacement for each photograph was applied to the rigid upper plate. The contact algorithm then determined the total compression force at equilibrium. Friction and adhesion effects were neglected.

2.7. *Inverse modeling procedure*

The difference γ_W between the work done on the lens by the compression apparatus experimentally, W_E, and that predicted by the model, W_M, was computed as

$$\gamma_W = \int |F_E - F_M| d\delta,$$

where F_E and F_M are the forces observed experimentally and computed by the model, respectively. This integral was computed using the trapezoid rule based on the force F and displacement δ measurements from the retained points in increments of $\sim$2.5% compression.

Initial attempts for inverse modeling minimized γ_W by varying the mechanical properties in the model to determine which combination would optimally predict the experimental force–displacement curve. However, we later determined that this result was not unique and the resulting "optimum" depended heavily on the initial guesses chosen for the shear moduli. Therefore, an elastographic approach was adopted in which the geometry of the experimental and computational lenses was compared at each load step (Fig. 4). The approach is

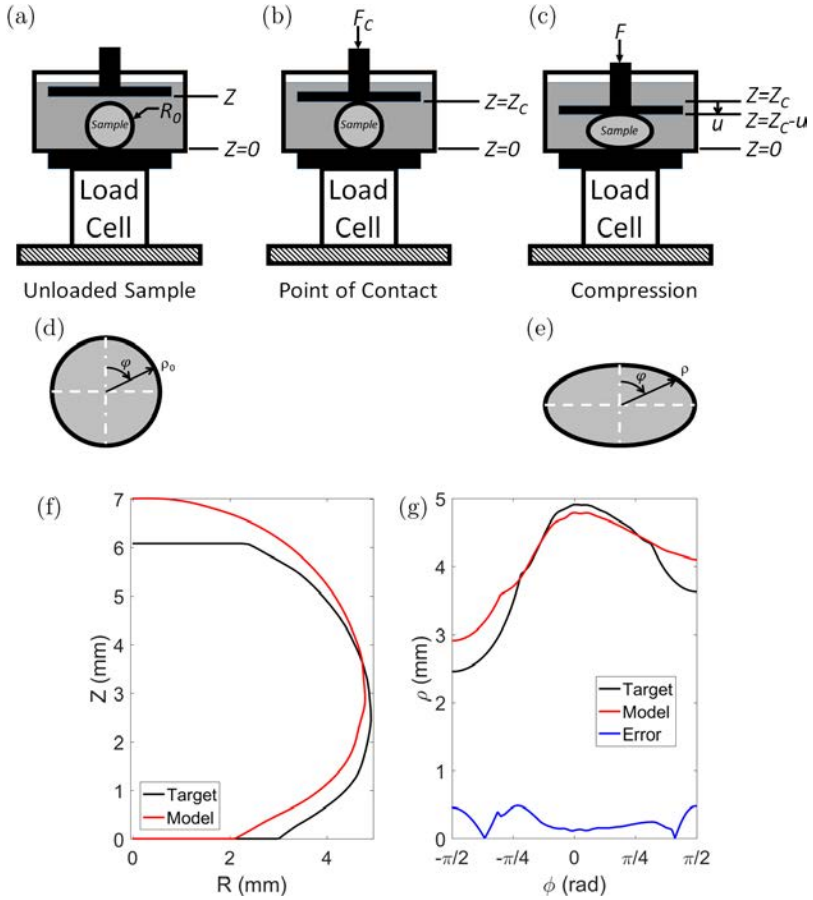

Fig. 4. Above: Schematic of the lens compression test. (a) Prior to contact, the zero gap is established and the lens photographed, (b) then, contact is established, setting the initial force and position, and (c) the lens is compressed by a load F to an extent δ. The lens' cross-sectional profile is determined for (d) the initial geometry (defined as $\rho_0(\varphi)$) and (e) the loaded geometry ($\rho(\varphi)$). Below: Example of the comparison for a decapsulated porcine lens in Cartesian (f) and polar (g) coordinates.

based on that described by Burd *et al.*[8] wherein a target outline ρ_T derived from experiments is compared to the model-predicted outline ρ_M. The absolute value of the difference in distances from the center of the lens to the surface was integrated with respect to the polar angle φ from the posterior pole to the anterior pole. This yielded an error in cross-sectional area $A_{E,i}$ which was then normalized against the entire cross-sectional area of the experimental (target) geometry for the corresponding ith load step $A_{T,i}$ to give a fractional area error metric $\gamma_{A,i}$:

$$\gamma_{A,i} = \frac{A_{E,i}}{A_{T,i}} = \frac{\int_{-\frac{\pi}{2}}^{\frac{\pi}{2}} |\rho_T^2 - \rho_M^2| d\phi}{\int_{-\frac{\pi}{2}}^{\frac{\pi}{2}} \rho_T^2 d\phi}.$$

Since both of these error metrics should be minimized in an ideal solution, this is a multi-objective optimization problem. An overall weighted error metric Γ was therefore computed by adding γ_W and summing $\gamma_{A,i}$ over all N compression increments as

$$\Gamma = 0.001\gamma_W + \frac{1}{N}\sum_{i=1}^{N} \gamma_{A,i}.$$

Note that γ_W can take on extremely large values in some cases where the input lens shear modulus is very high, so this term was assigned a small fractional weight to avoid overwhelming the area error term. This weight was somewhat arbitrarily selected but it did not significantly influence the optimal values. Indeed, it was noted that the errors in work and cross-sectional area tended to vary quite differently with the parameters (e.g., Fig. 5). The area error term was weighted by the inverse of N to allow comparison of results from experiments which include varying numbers of loading increments.

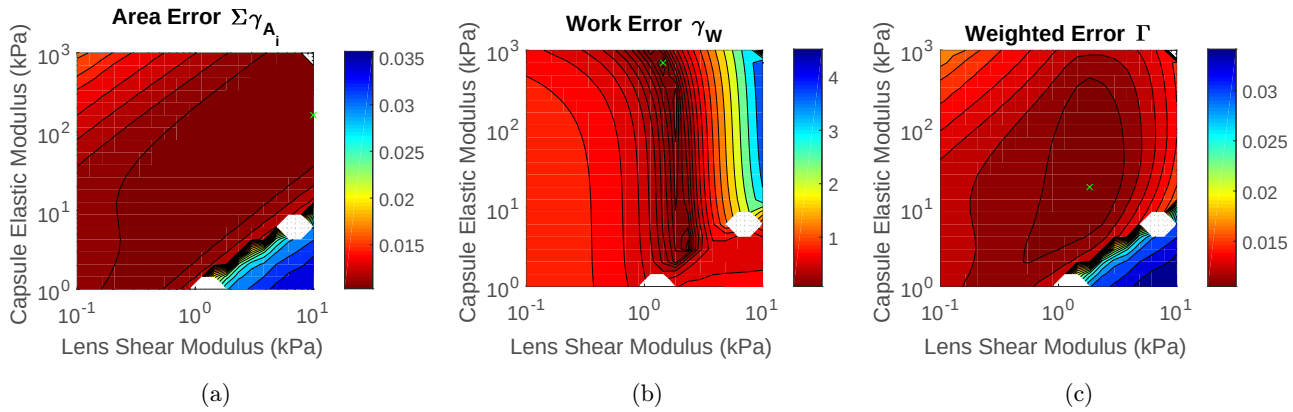

Fig. 5. Contour plots showing the relative error in fitting (a) cross-sectional area ($\Sigma\gamma_{A,i}$), (b) work γ_W, and (c) the weighted error metric Γ combining the two for the decapsulated porcine lens as a function of lens shear modulus G_{lens} (x-axis) and capsule elastic modulus E_{capsule} (y-axis). The work error is minimized for infinitely many combinations of G_{lens} and E_{capsule}, indicating that simply fitting the force–displacement curve will not yield unique values for mechanical properties.

The mechanical parameters describing the model were then determined by minimizing Γ. In practice, this was accomplished using a multi-step algorithm. For the decapsulated lens, 20 log-spaced values of shear modulus were evaluated while holding $\kappa = 100\,\text{G}$. For the encapsulated lens, a 20× 20-point log-spaced gridded search was completed using the lens shear modulus and capsule elastic modulus for the encapsulated lens while holding $\kappa = 100\,\text{G}$. The range of shear modulus values considered in this grid scan was 0.1–10 kPa for porcine lens shear modulus, 1–100 kPa for murine lens shear modulus, and 0.01–10 MPa for the elastic modulus of the capsule. The parameter set which minimized Γ on this grid was used as an initial guess when optimizing with the Nelder–Mead simplex optimization method[45] as implemented in the *fminsearch*() function in MATLAB. In each iteration, updated values for the mechanical properties were specified, the model solved, and Γ calculated.

3. Results

Table 1 gives the stiffness, lens shear modulus, and capsule elastic modulus estimates for each lens. The presence of the lens capsule increased the extrinsic stiffness and Hertz shear modulus of the porcine lens by about 55%, indicating that its role cannot be neglected. The murine lens and its capsule were far stiffer than the porcine lens: its extrinsic stiffness was about 42% higher than the encapsulated porcine lens while its shear modulus was over fourfold higher. This disparity demonstrates the importance of using intrinsic mechanical properties to accurately compare lenses by accounting for lens size and shape.

The lens compression test yielded values for the porcine lens shear modulus which were broadly in line with previous experiments. The inverse FE analysis results indicated an optimal value of 0.672 kPa. The incompressibility assumption (i.e., $\kappa = 100\,\text{G}$) was justified on the basis of another grid scan for the decapsulated lens in which both G and κ were varied (Fig. 6). Since the reported value of κ for the porcine lens is 2.5–3.0 GPa,[46] the optimal value of G is effectively independent of κ as long as the κ/G ratio exceeds 100. This approach was previously adopted by Burd *et al.*, who fixed the ratio of bulk modulus to shear modulus at 100 for all simulations.[8] This is important because very large values for the

Table 1. Stiffness and shear modulus estimates.

	Extrinsic stiffness (mN/mm)		Shear modulus (kPa)			
Lens	Linear (≤ 10%)	Exponential	FE model	Hertz	Rel. error	E_{capsule} (kPa)
Decapsulated porcine	4.98	4.63–11.9	0.672	0.615	−8.5%	—
Encapsulated porcine	7.73	7.17–18.5	2.05	0.958	−53.2%	20.08
Encapsulated murine	10.98	11.9–14.4	8.849	6.266	−29.2%	6420

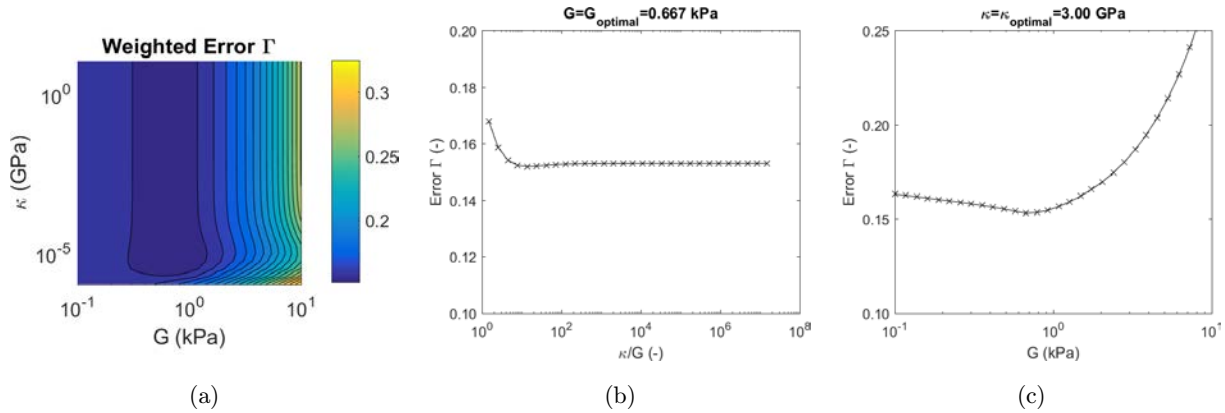

(a) (b) (c)

Fig. 6. Effects of shear modulus G and bulk modulus κ of the decapsulated porcine lens. (a) Contour plot showing the fitting error as a function of G and κ. Contours are parallel to the κ-axis for all realistic values of κ, indicating its precise value is unimportant in determining the model predictions. (b) The error decreases as κ increases for constant G. Specifically, a ratio κ/G of greater than 100 yields no appreciable improvement in the solution. (c) At a realistically high value of κ, the approach yields an optimum for G of 0.667 kPa.

bulk modulus can cause numerical difficulties in the FE method due to the Poisson locking effect.[49]

Stress and strain distributions were computed for each lens. Figure 7 shows the distribution for the decapsulated porcine lens though distributions computed for other lenses were generally similar in appearance. Significant stress concentrations were observed in the vicinity of the initial edge of

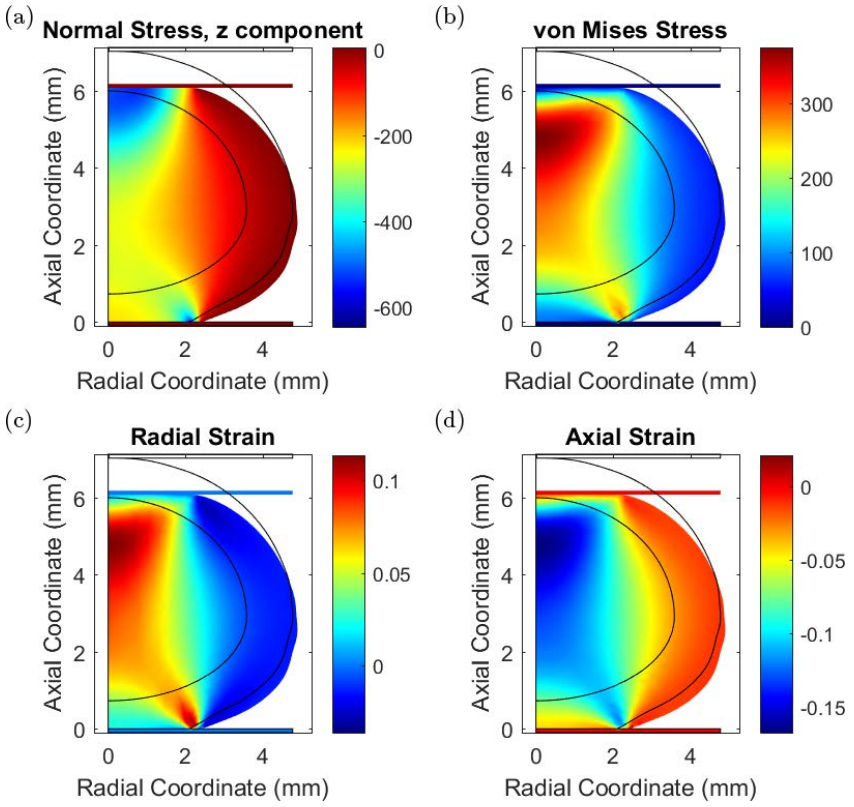

Fig. 7. Spatial variation of (a, b) stress and (c–f) strain within the Model A (homogeneous) decapsulated porcine lens at 15% compression. Note that the stress and strain are very heterogeneous throughout the lens. In general, the maximum value of the axial strain within the lens was similar to the applied fractional compression. However, stresses and strains varied significantly through the lens.

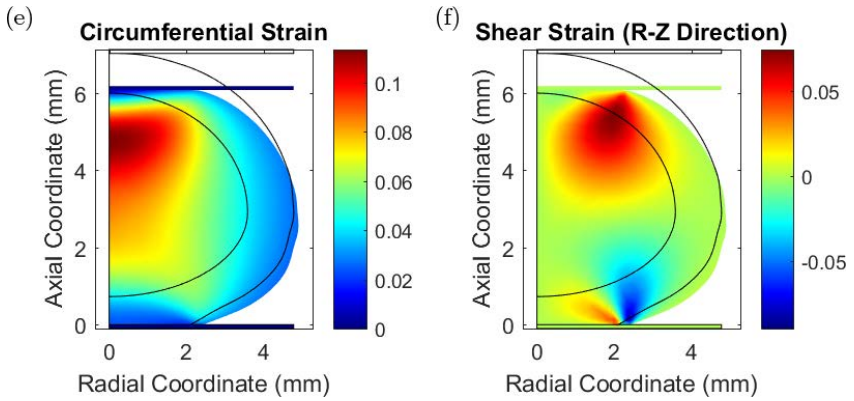

Fig. 7. (*Continued*)

contact, possibly owing to the assumption that friction and adhesion were negligible.

4. Discussion

The compression testing protocol and computational methods described above offer a novel method for comparing the intrinsic mechanical properties of lenses from different genotypes regardless of size or other differences. Measurements on both porcine and murine lenses indicate good agreement with previous measurements of extrinsic lens stiffness reported by other groups. Our estimates for the porcine lens shear modulus and capsule elastic modulus are in line with the previously-reported values, and we report the first estimate of these parameter values for the murine lens and capsule.

This is the first application of an inverse modeling approach to allow an estimation of the intrinsic mechanical properties of the lens from a compression test. This approach borrows heavily from the method developed by Burd *et al.* for lens spinning.[8] While simply matching the model's predicted force–displacement curve to the experimental values is far easier, a preliminary study found that this approach did not provide a unique optimal pairing of modulus values. This may be seen in Fig. 5 by observing that the values of the work and area errors are optimized for infinitely many pairs of modulus values. However, by combining and weighting these two metrics, unique modulus values were achieved.

All lenses exhibited nonlinear force–displacement behavior consistent with the Hertzian contact theory[35,36] wherein the force increased with the displacement to the 3/2 power. Shear modulus values determined in this manner were broadly in line with the previous measurements. Importantly, the presence of the lens capsule in the porcine lens inflates its extrinsic stiffness and its Hertz model-estimated shear modulus by about 55%. These results were generally in agreement with the results of the inverse FE analysis, which also assumed that the lens is mechanically homogeneous. The Hertz model can therefore be used as a first approximation for decapsulated lenses, but falls short when encapsulated lenses are considered. It also fails to account for spatial variations of the shear modulus within the lens (as does the present FE-based approach). Still, it is an improvement upon using a linear regression of the force–displacement curve since it gives an idea of the intrinsic mechanical properties by accounting for the lens' radius of curvature.

4.1. *Comparison with the literature measurements*

Estimates of the extrinsic stiffness of lenses were broadly in line with the literature values (Table 1). Sharma *et al.* fitted a line to a portion of the loading data from a rapid compression of pig lenses, yielding an apparent stiffness of ∼150 mN/mm.[22] This disparity is presumably due to the use of the high strain rate portion of the data. Analysis of their fully relaxed force data yields a stiffness of 4.6 mN/mm which is very similar to our 4.98 mN/mm.

Linear stiffness values for adult wild-type murine lenses range from 5–50 mN/mm,[23–25,27] whereas we measured ∼11 mN/mm. Our own measurement of 11.9 mN/mm at low extents of compression is similar to the measurements of 12.4 mN/mm by Gokhin *et al.* at 6% compression.[25] Extrapolation indicates that, if our experiments had achieved 27% compression, the exponential stiffness would have been 22.0 mN/mm whereas Gokhin *et al.* measured 27.6 mN/mm. This gives confidence that the methods used to generate force–displacement data and subsequently estimate the extrinsic stiffness of the lens are reliable.

The shear modulus of the porcine lens is similar to that reported previously by Reilly and Ravi.[12] The estimated elastic modulus of the porcine lens capsule was somewhat lower than those reported previously using two distinct methods.[31,47] This is likely due to the disparity in methodologies applied while assuming that the capsule is accurately represented by a linearly elastic material. Burd and Regueiro have shown that a microstructural membrane model accurately describes the published mechanical data for the lens capsule generated by using multiple.[48] Incorporation of a more appropriate constitutive model for the lens capsule may significantly improve the proposed method.

The optimized value for the murine shear modulus was 8.85 kPa — roughly similar to the lens of a 60-year-old human.[38] The elastic modulus of the murine lens capsule is 6.42 MPa — far higher than previously-reported values for other species. To our knowledge, this is the first time that the elastic modulus of the murine lens or capsule has been reported in the literature.

4.2. *Limitations*

Preliminary studies attempted to estimate the mechanical properties by simply matching the experimentally-determined force–displacement curves. Unfortunately, this approach does not yield a unique solution (Fig. 5) and was therefore abandoned. In its place, we have developed an inverse FE approach which compares the geometry of the experimental and computational lenses to ensure uniqueness in estimating the mechanical properties of the lens. Most of the steps in this process have now been automated and it is readily applicable to lenses of any species.

The FE model assumed that the lens was accurately described by a uniform, isotropic, neo-Hookean material model. This implicitly neglects any porous or viscous effects as well as known spatial variations in lens properties (e.g., Ref. 12). Investigation into the true constitutive mechanical behavior of the lens will require additional theoretical developments, more advanced FE analysis, and additional experiments in which loading rate effects are included as a parameter. Future work will work toward overcoming these assumptions to give a more realistic picture of the lens' mechanical behavior.

The lens volume was calculated, using numerical integration, from photographs of the compression experiments by assuming that the lens was axisymmetric and remained so throughout loading. This is indicating a volume change of less than 0.5% at 15% compression in all cases, which may be within the resolution of the method used to estimate the volume. This does not imply that the lens volume does not change during accommodation as there are several key differences between these mechanical loadings. For example, the timescale of accommodation is much shorter (i.e., the loading rate, which contributes to viscous fluid flow, is much higher) and the compression test decreases capsule surface area available for fluid flow. Thus, the compression test is not a useful way to determine whether lens volume changes during accommodation.

4.3. *Conclusions*

In summary, we have established a method for estimating the mechanical properties of lenses of considerably different shapes, sizes, and mechanical properties. This approach is comprised of a simple mechanical test which may be used to perform lens--specific inverse FE analysis. Future work will incorporate automated loading protocols for rate-dependent testing spatial variations in lens mechanical properties in the analysis. These methods will then be applied to the study of murine and human lenses to improve our understanding of the mechanisms underlying age-related mechanical changes in the lens.

References

1. A. Gullstrand, *Helmholtz's Treatise on Physiological Optics*, translated edition, The Optical Society of America, New York (1924).

2. J. F. Koretz, G. H. Handelman, "How the human eye focuses," *Sci. Am.* **259**, 92–99 (1988).
3. M. A. Reilly, "A quantitative geometric mechanics lens model: Insights into the mechanisms ofaccommodation and presbyopia," *Vision Res.* **103**, 20–31 (2014).
4. R. F. Fisher, "The significance of the shape of the lens and capsular energy changes inaccommodation," *J. Physiol.* **201**, 21–47 (1969).
5. R. A. Weale, On potential causes of presbyopia, *Vision Res.* **39**, 1263–1272 (1999).
6. H. J. Burd, S. J. Judge, J. A. Cross, "Numerical modelling of the accommodating lens," *Vision Res.* **42**, 2235–2251 (2002).
7. R. F. Fisher, "The elastic constants of the human lens," *J. Physiol.* **212**, 147–180 (1971).
8. H. J. Burd, G. S. Wilde, S. J. Judge, "An improved spinning lens test to determine the stiffness of the human lens," *Exp. Eye. Res.* **92**, 28–39 (2011).
9. M. A. Reilly, P. Martius, S. Kumar, H. J. Burd, O. Stachs, "The mechanical response of the porcinelens to a spinning test," *Z. Med. Phys.* **26**, 127–135 (2016).
10. H. A. Weeber, G. Eckert, F. Soergel, C. H. Meyer, W. Pechhold, R. G. L. van der Heijde, "Dynamic mechanical properties of human lenses," *Exp. Eye. Res.* **80**, 425–434 (2005).
11. H. A. Weeber, E. Gabriele, P. Wolfgang, "Stiffness gradient in the crystalline lens," *Graefes Arch. Clin. Exp. Ophthalmol.* **245**, 1357–1366 (2007).
12. M. A. Reilly, R. Nathan, "Microindentation of the young porcine ocular lens," *J. Biomech. Eng.* **131**, 44502 (2009).
13. K. R. Heys, C. S. Leigh, T. R. J. Willis, "Massive increase in the stiffness of the human lens nucleuswith age: The basis for presbyopia?" *Mol. Vis.* **10**, 956–963 (2004).
14. S. T. Bailey, M. D. Twa, J. C. Gump, M. Venkiteshwar, M. A. Bullimore, R. Sooryakumar, "Light-scattering study of the normal human eye lens: Elastic properties and age dependence," *IEEE Trans. Biomed. Eng.* **57**, 2910–2917 (2010).
15. J. Randall, J. M. Vaughan, "The measurement and interpretation of Brillouin scattering in the lens of the eye," *Proc. R. Soc. Lond. B, Biol. Sci.* **214**, 449–470 (1982).
16. S. Reiss, O. Stachs, R. Guthoff, H. Stolz, "Non-invasive, spatially resolved determination of tissue properties of the crystalline lens with regard to rheology, refractive index, densityand protein concentration by using Brillouin spectroscopy," *Klin. Monbl. Augenheilkd.* **228**, 1079–1085 (2011).
17. G. Scarcelli, P. Kim, S. H. Yun, "*In vivo* measurement of age-related stiffening in the crystalline lens by Brillouin optical microscopy," *Biophys. J.* **101**, 1539–1545 (2011).
18. G. Scarcelli, S. H. Yun, "*In vivo* Brillouin optical microscopy of the human eye," *Opt. Express* **20**, 9197–9202 (2012).
19. J. M. Vaughan, J. T. Randall, "Brillouin scattering, density and elastic properties of the lens and cornea of the eye," *Nature* **284**, 489–491 (1980).
20. S. Yoon, S. Aglyamov, A. Karpiouk, S. Emelianov, "The mechanical properties of *ex vivo* bovine and porcine crystalline lenses: Age-related changes and location-dependent variations," *Ultrasound Med. Biol.* **39**, 1120–1127 (2013).
21. T. N. Erpelding, K. W. Hollman, M. O'Donnell, "Mapping age-related elasticity changes in porcine-lenses using bubble-based acoustic radiation force," *Exp. Eye Res.* **84**, 332–341 (2007).
22. P. K. Sharma, H. J. Busscher, T. Terwee, S. A. Koopmans, T. G. van Kooten, "A comparative study on theviscoelastic properties of human and animal lenses," *Exp. Eye Res.* **93**, 681–688 (2011).
23. H. Baradia, N. Negin, G. Adrian, "Mouse lens stiffness measurements," *Exp. Eye Res.* **91**, 300–307 (2010).
24. C. Cheng, D. S. Gokhin, R. B. Nowak, V. M. Fowler, "Sequential application of glass coverslips to assess the compressive stiffness of the mouse lens: Strain and morphometric analyses," *J. Vis. Exp.* **111**, e53986 (2016).
25. D. S. Gokhin, R. B. Nowak, N. E. Kim *et al.*, "Tmod1 and CP49 synergize to control the fiber cell geometry, transparency, and mechanical stiffness of the mouse lens," *PLoS One* **7**, e48734 (2012).
26. G. J. Won, D. S. Fudge, V. Choh, "The effects of actomyosin disruptors on the mechanical integrity of the avian crystalline lens," *Mol. Vis.* **21**, 98–109 (2015).
27. D. S. Fudge, J. V. McCuaig, S. Van Stralen *et al.*, "Intermediate filaments regulate tissue size and stiffness in the murine lens," *Invest. Ophthalmol. Vis. Sci.* **52**, 3860–3867 (2011).
28. R. F. Fisher, "Elastic constants of the human lens capsule," *J. Physiol.* **201**, 1–19 (1971).
29. M. R. Heistand, R. M. Pedrigi, S. L. Delange, J. Dziezyc, J. D. Humphrey, "Multiaxial mechanical behavior of the porcine anterior lens capsule," *Biomech. Model. Mechanobiol.* **4**, 168–177 (2005).
30. G. Wollensak, E. Spoerl, "Influence of indocyanine green staining on the biomechanical properties of porcine anterior lens capsule," *Curr. Eye Res.* **29**, 413–417 (2004).
31. S. Krag, T. T. Andreassen, "Biomechanical measurements of the porcine lens capsule," *Exp. Eye Res.* **62**, 253–260 (1996).

32. Y. Shi, "Further analysis of the lens phenotype in Lim2-deficient mice," *Invest. Ophthalmol. Vis. Sci.* **52**, 7332–7339 (2011).
33. M. D. Perng, R. A. Quinlan, "Seeing is believing! The optical properties of the eye lens aredependent upon a functional intermediate filament cytoskeleton," *Exp. Cell Res.* **305**, 1–9 (2005).
34. U. P. Andley, A. Reilly Matthew, "*In vivo* lens deficiency of the R49C alphaA-crystallin mutant," *Exp. Eye Res.* **90**, 699–702 (2010).
35. H. Hertz, "Ueber die Berührung fester elastischer Körper," *J. Reine Angew. Math.* **92**, 156–171 (1882).
36. K. L. Johnson, "One hundred years of hertz contact," *Proc. Inst. Mech. Eng.* **196**, 363–378 (1982).
37. S. Bassnett, H. Šikić, "The lens growth process," *Prog. Retin. Eye Res.* **60**, 181–200 (2017).
38. G. S. Wilde, H. J. Burd, S. J. Judge, "Shear modulus data for the human lens determined from aspinning lens test," *Exp. Eye Res.* **97**, 36–48 (2012).
39. C. K. Chai, H. J. Burd, G. S. Wilde, "Shear modulus measurements on isolated human lens nuclei," *Exp. Eye Res.* **103**, 78–81 (2012).
40. N. Ravi, K. T. Wan, K. Swindle, P. D. Hamilton, G. Duan, "Development of techniques to comparemechanical properties of reversible hydrogels with spherical, square columnar, and ocular lens geometry," *Polymer* **47**, 4203–4209 (2006).
41. M. A. Reilly, D. Hamilton Paul, R. Nathan, "Dynamic multi-arm radial lens stretcher: A robotic analog of the ciliary body," *Exp. Eye Res.* **86**, 157–164 (2008).
42. M. A. Reilly, D. Hamilton Paul, P. Gavin, R. Nathan, "Comparison of the behavior of natural and refilled porcine lenses in a robotic lens stretcher," *Exp. Eye Res.* **88**, 483–494 (2009).
43. M. A. Reilly, U. P. Andley, "Quantitative biometric phenotype analysis in mouse lenses," *Mol. Vis.* **16**, 1041–1046 (2010).
44. B. P. Danysh, K. J. Czymmek, P. T. Olurin, J. G. Sivak, M. K. Duncan, "Contributions of mouse genetic background and age on anterior lens capsule thickness," *Anat. Rec. (Hoboken)* **291**, 1619–1627 (2008).
45. J. C. Lagarias, J. A. Reeds, M. H. Wright, P. E. Wright, "Convergence properties of the Nelder–Mead simplex method in low dimensions," *SIAM J. Optimiz* **9**, 112–147 (1998).
46. S. Reiss, K. Sperlich, M. Hovakimyan *et al.*, "*Ex vivo* measurement of postmortem tissue changes in the crystalline lens by Brillouin spectroscopy and confocal reflectance microscopy," *IEEE Trans. Biomed. Eng.* **59**, 2348–2354 (2012).
47. T. A. Powell, R. Amini, A. Oltean *et al.*, "Elasticity of the porcine lens capsule as measured by osmotic swelling," *J. Biomech. Eng.* **132**, 91008 (2010).
48. H. J. Burd, R. A. Regueiro, "Finite element implementation of a multiscale model of the human lens capsule," *Biomech. Model. Mechanobiol.* **14**, 1363–1378 (2015).
49. B. Szabo, I. Babuska, *Finite Element Analysis*, John Wiley & Sons, New York (1991).